Reaction ^{2}H(p,dπ^+)n at 506 MeV

B. Debebe,* C. F. Perdrisat, and V. Raghunathan†
Physics Department, College of William and Mary, Williamsburg, Virginia 23185

J. M. Cameron, I. J. van Heerden,‡ P. Kitching,§ R. MacDonald,** W. J. McDonald, W. C. Olsen, J. Soukup, and H. S. Wilson††
Nuclear Research Centre, University of Alberta, Edmonton, Alberta, Canada T6J 2J1

H. W. Fearing and C. A. Miller
TRIUMF, Vancouver, British Columbia, Canada V6T 1W5
(Received 19 December 1984)

Differential cross sections for the reaction ^{2}H(p,dπ^+)n have been obtained at 506 MeV. The deuteron angles were 11°, 13°, 15°, and 17°, and the pions were detected at 14 angles between 24° and 96°. The data, covering the region of neutron recoil momenta 10 to 140 MeV/c, are analyzed using the plane-wave impulse approximation to extract a momentum density of the proton in the deuteron. Systematic deviations from the plane-wave impulse approximation prediction are interpreted on the basis of a simplified calculation of the nd rescattering cross section.

I. INTRODUCTION

Among the proton induced reactions leading to production of a single pion from a light nucleus, ^{2}H(p,dπ^+)n is the simplest next to the fundamental pp$\rightarrow$dπ^+ process. The two-body pion production (p,π^+), and the absorption channel (π^+,p) have been investigated extensively, in part because they involve very large momentum transfers $\mathbf{q}=\mathbf{p}_p-\mathbf{p}_\pi$, and therefore large internal momenta in the target nucleus, assuming they occur predominantly in a one-step process. For example, with 500 MeV protons, $q>700$ MeV/c in ^{2}H(p,dπ^+)n, and at threshold $q\cong 600$ MeV/c. However, relative little direct information about the large internal momentum content of nuclear wave functions has been obtained from the interpretation of (p,π^+) or (π^+,p) cross sections and asymmetry data because multinucleon processes are always important, sometimes dominant. Several approaches to calculate the observables of two-body pion production have been used, with results that are often nontrivially different. Fearing[1] and Walden[2] have recently reviewed model calculations and the present experimental situation for (p,π^+).

In contrast with the situation for two-body (p,π), the ^{2}H(p,dπ^+)n reaction can proceed in the quasi-free (QF) mode, with no (or small) internal momentum q required. In the impulse approximation (IA), and for the one-step Feynman diagram in Fig. 1(a), $\mathbf{q}=-\mathbf{p}_5$, where $\mathbf{p}_5$ is the recoil momentum of the (unobserved) neutron in the laboratory frame. However, even for small p_5 values, other processes possibly contribute. Figures 1(b) and (c) show two-step diagrams which are expected to become increasingly important at large neutron recoil momenta. Yet, for small neutron recoil momenta there is experimental evidence, from ^{2}H(p,2p)n in particular,[3] that these rescattering processes contribute relatively small corrections to the IA diagram of Fig. 1(a). The ^{2}H(p,dπ^+)n reaction is particularly interesting because it provides a unique opportunity to study the pion production process in the IA regime with pion-nucleon rescattering [Fig. 1(c)] quenched by isospin conservation. The (π^+n) pair must be in the isospin $\frac{1}{2}$ state because of the isoscalar nature of the deuteron. The strong, resonating isospin $\frac{3}{2}$ (πN) interaction is thus not present, leading one to expect that an nd rescattering correction to the IA might be sufficient to explain the data.

Five independent kinematic variables are necessary to completely describe the final state dπ^+n. Thus the magnitude p_5 of the recoil does not define the final state uniquely; one is free to choose four more variables. For example, one can choose the polar and azimuthal angles of the recoil momentum (θ_5,φ_5) and the total energy of the dπ pair which regulates the pp$\rightarrow$dπ vertex in Fig. 1(a). Alternatively, one can describe the final state with a

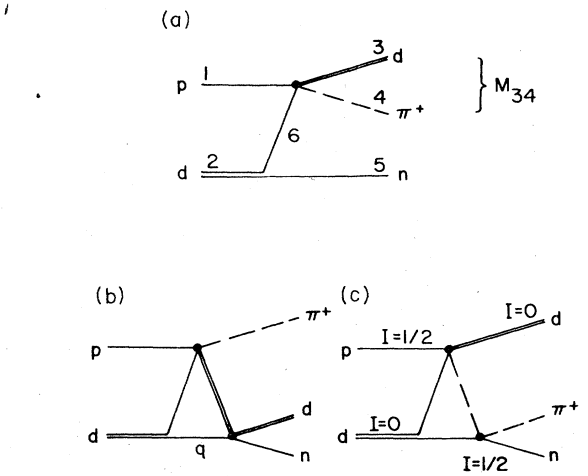

FIG. 1. The three processes considered are the impulse approximation (a), nd rescattering (b), and π^+n rescattering (c).

combination of variables taken from the three pairwise kinetic energies T_{ij} and the six invariant momentum transfers squared $t_{1j}=(p_1-p_j)^2$ and $u_{2j}=(p_2-p_j)^2$, where the p's are four-vectors and participants are numbered 2(1,34)5. If one wishes to use exclusively invariant quantities, one can choose one or several of the pairwise invariant masses squared $M_{ij}^2=(p_i+p_j)^2$ instead of the relative energies T_{ij}. Each one of these quantities can be calculated from the five directly measured, which in the present experiment were $\mathbf{p}_3(p_3,\theta_3,\varphi_3)$ and (θ_4,φ_4). Some of these variables are particularly relevant to the study of rescattering processes like those in Figs. 1(b) and (c). For example, M_{35} regulates the nd rescattering amplitude in Fig. 1(b); nd rescattering will be most important when $M_{35}\sim m_n+m_d$. Likewise, M_{45} is one of the two variables controlling the πn scattering amplitude in Fig. 1(c).

Again because by itself the recoil momentum does not specify the final state, the reaction can be investigated at fixed recoil for ranges of values of the other variables of interest. The present experiment was designed to provide as large a range of values of M_{45} and M_{35} (or alternately t_{14}) as possible for a range of recoil momenta, with the expectation that such data would provide the empirical basis for a study of the contribution of processes like pion or deuteron rescattering. The range of neutron recoil momenta investigated in the experiment is limited to 10 to 146 MeV/c. The deuteron wave function is well known for the relatively small internal momenta required under these conditions.

The data presented below show systematic and significant deviations from a plane wave impulse approximation (PWIA) prediction already for small neutron recoil momenta, and for deuteron angles close to the QF region. Typically, the momentum-space density, $|\phi|^2$, for a proton in the deuteron calculated in the PWIA does not have a unique value for a given neutron recoil, contrary to expectation for the diagram of Fig. 1(a). The $|\phi|^2$ data tend to cluster along a looping locus, larger $|\phi|^2$ values being the rule for large pion angles, and smaller $|\phi|^2$ values for small pion angles. A simplified calculation of the nd rescattering contribution using the method of Laget[4] explains qualitatively this double valuedness in $|\phi|^2$ in terms of forward and backward rescattering, although no quantitative agreement with the data is achieved.

The novelty of the data presented here is thus a systematic exploration of the phase space available to the three final state particles. Only one other counter experiment was carried out with a similar goal in mind: that of Lo *et al.*[5] for the same reaction at 800 MeV. The number of different data points in the final state phase space is however more than an order of magnitude larger in the present experiment than in Ref. 5. However, the statistical accuracy per data point in the present work is not as good as in Ref. 5. The same reaction has also been studied at 585 MeV by Hogstrom *et al.*,[6] but only in geometries with $p_5>400$ MeV/c. In a subsequent analysis of these data, Duck *et al.*[7] found, using the Glauber theory, that the largest contribution to the cross section at these large neutron recoil momenta comes from double scattering.

The experiment is described in Sec. II, and the data analysis in Sec. III. The results are presented in Sec. IV and discussed in Sec. V, where the results of the nd rescattering calculation are also shown. Section VI contains the conclusions.

II. DESCRIPTION OF THE EXPERIMENT

The complete description of a three-body final state requires the experimental determination of 12 kinematical variables, i.e., three four-vectors. If, however, the invariant masses of the three final state particles are determined independently, four-momentum conservation reduces the list of kinematical variables to be measured to five. In this experiment the deuteron momentum vector $\mathbf{p}_3(p_3,\theta_3,\varphi_3)$ and the pion angles (θ_4,φ_4) were determined for each event.

A. Apparatus

The experiment was performed at the TRIUMF facility, using a 506 MeV external proton beam. A schematic diagram of the apparatus is shown in Fig. 2. The medium resolution spectrometer (MRS) on the left-hand side of the beam was used to detect deuterons from the reaction ^{2}H(p,dπ^+)n. Proton contamination in the MRS was eliminated in the subsequent data analysis by placing cuts on the time of flight (TOF) between counters *SL* 1 and *SL* 2, separated by 9 m, and on the pulse height (PH) in these counters. The MRS was positioned at four angles from 11° to 17° in steps of 2°. At each angle, three values of magnetic field were used to cover the range of interesting deuteron momenta, also providing for momentum acceptance overlap. The usable momentum acceptance was found to be ±12% of the central momentum. The MRS was equipped with three multiwire proportional chambers (MWPC) each providing an x- and a y-coordinate for the trajectory of a particle. The first MWPC was located in front of the entrance quadrupole singlet Q, while the other two were on either side of the focal plane, 100 cm apart. The quadrupole focuses in the horizontal plane, and the dipole, which bends particles upward, focuses in the vertical (the momentum analyzing) plane. The left-hand solid angle was determined by the size of *SL* 1, but the final solid angle of 0.99 msr was defined with cuts on the front MWPC coordinates during data analysis.

Pions were detected in 14 two-counter telescopes positioned between 24° and 96° on the right-hand side of the beam, with the first nine at 4° intervals and the rest at 8° intervals. In each of the two-counter telescopes, the front detector *SR* 1 was a 0.32 cm thick circular plastic scintillator of diameter 12.7 cm. The back detector *SR* 2 was a cylindrical plastic scintillator 7.62 cm thick of diameter 11.4 cm, located 5 cm behind *SR* 1. Four of the first nine telescopes were 4.3° above the horizontal plane, while five were below by the same amount, in an alternating pattern. The distance from the target to *SR* 2, was 150 cm. Each telescope subtended a solid angle of 4.54 msr defined by *SR* 2. No MWPC were used on this side, and thus the data were averaged over the circular acceptance of ±2.2°.

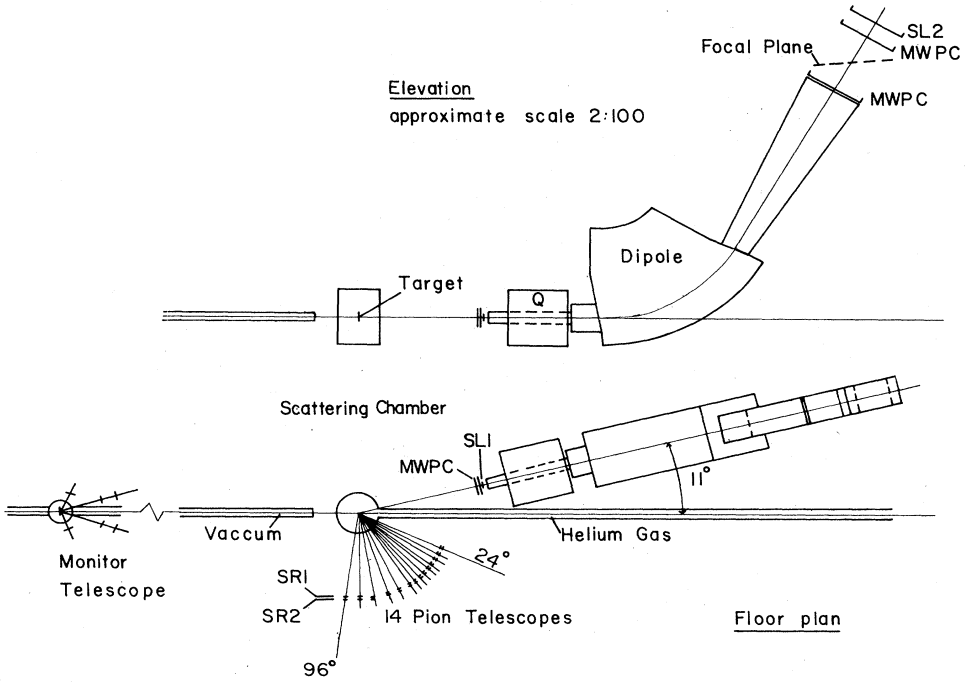

FIG. 2. Elevation and floor plan of the experiment showing the medium resolution spectrometer (MRS) and the 14 pion telescopes.

B. Beam, targets, and monitors

Beam currents used in this experiment were between 1 and 2 nA. The energy resolution of the beam is typically 1 MeV full width at half maximum (FWHM), and the nominal value of the energy of 506 MeV is known to ± 1 MeV. The beam divergence and spot size at the target position were found to be approximately ± 0.2 mrad and 0.25 cm^2, respectively. The beam position at the target was monitored frequently by observing the spot on a fluorescent screen inserted temporarily at the target location.

The targets used in this experiment were a 210 $mg\,cm^{-2}$ CD_2 foil and a 195 $mg\,cm^{-2}$ C foil. The data from the carbon target were used for the subtraction of background events. These targets were mounted on a remotely controlled ladder oriented at 36° to the right of the beam.

Two conjugate sets of two-arm telescopes viewing a 5 $mg\,cm^{-2}$ thick secondary CH_2 target located 11 m upstream from the primary target were used as flux monitors. The telescopes were positioned to be sensitive to pp scattering at 17° in the laboratory frame on either side of the beam. Both telescopes were calibrated prior to data taking by comparison with a Faraday cup. Accidental events were also counted as delayed coincidences and subtracted.

C. Electronics and data acquisition technique

The standard event selection electronics and the computer interfacing of the MRS have been described elsewhere.[8] The additional electronic logics necessitated by the addition of 14 pion telescopes is shown schematically in Fig. 3. The "Master AND" circuit senses a coincidence between short pulses from the *SL* 1 detector and the MRS side, and a wide gate pulse generated whenever one of the pion telescopes detected a particle. The function of the "Latching OR" circuit in Fig. 3 is to prevent any coincidence event from being accepted before either the current event is fully processed, or in the absence of an MRS validation signal, a fast reset signal is generated.

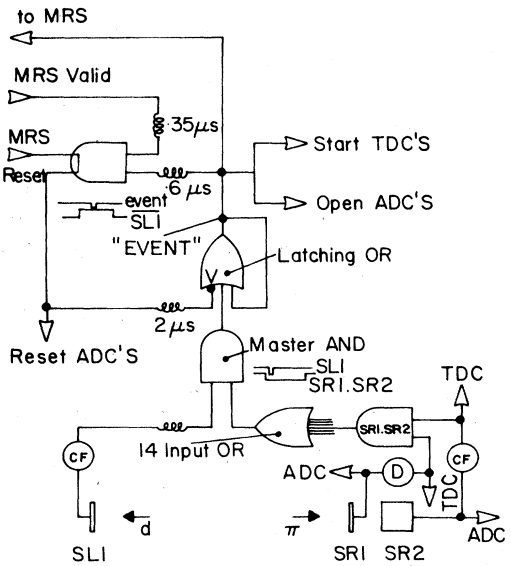

FIG. 3. Block diagram of the electronics used to detect left-right coincidences between signals from the front counter *SL* 1 and one of the pion telescope (*SR* 1.*SR* 2).

For valid events, the digitized amplitudes of pulses from all scintillators (ADC) and digitized times from *SL* 1 to all fourteen *SR* 1 and *SR* 2 detectors [time-to-digital converters (TDC)] were stored. A fraction of the events were analyzed on line, with the complete analysis done off line.

Random coincidences, for which the left- and right-hand side particles originated in two different beam bursts (which are 44.3 ns apart), were also collected. This sample of accidental events was then used in the data analysis to correct for accidental events originating from the same beam burst.

The combined electronics and computer dead time was monitored by feeding into the system "pulser" events triggering light-emitting diodes (LED) in each one of the scintillators. These events were generated randomly, but at a rate proportional to the incident proton flux, using accidental coincidences between monitor telescope pulses and a pulse generator operated at fixed frequency. The live time of the system was calculated as the fraction of pulser events accepted by the data acquisition system to the number of pulser triggers.

III. DATA ANALYSIS

Events obtained with the CD_2 and C targets were classified in intervals of the three independent, relativistically invariant kinematical variables s, t, and u calculated for each event from the measured quantities p_3,θ_3,φ_3 (MRS side) and the central values $\bar{\theta}_4,\bar{\varphi}_4$ of the pion telescope responsible for the event. The three invariant variables are defined below, where the complete definition of the cross section calculated from the data is also given. The relation to the PWIA is also presented and discussed, and the calculation of the single-proton internal momentum distribution is explained.

In terms of the five independent kinematical quantities directly measured in this experiment, the cross section is

$$\frac{d^3\sigma}{dp_3 d\Omega_3 d\Omega_4}=\frac{1}{\Delta p_3\Delta\Omega_3\Delta\Omega_4}\frac{N(\mathbf{p}_3,\theta_4,\varphi_4)}{nI\epsilon\epsilon_\pi}\ , \tag{3.1}$$

where $N(\mathbf{p}_3,\theta_4,\varphi_4)$ is the number of events registered within the intervals Δp_3, $\Delta\Omega_3$, and $\Delta\Omega_4$ around the values p_3, θ_3, φ_3, θ_4, and φ_4, after subtraction of accidental and carbon events. n, I, and ϵ are the number of protons on target, the number of deuterium nuclei per unit area of the target, and the overall efficiency including the live-time factor defined in Sec. II. ϵ_π is the pion decay loss factor.

Within the framework of the PWIA, the quantity of primary interest is p_5, the recoil momenta of the (unobserved) neutron, which is determined by the measurement of $\mathbf{p}_3$ and θ_4, φ_4 as follows: the total four-momentum for particle 4 and 5 together, M_{45} is obtained from

$$E_{45}=E_1+m_2-E_3=E_4+E_5\ ,$$

$$\mathbf{P}_{45}=\mathbf{p}_1-\mathbf{p}_3=\mathbf{p}_4+\mathbf{p}_5\ ,$$

$$M_{45}^2=E_{45}^2-P_{45}^2\ ;$$

then the pion momentum is a solution of a quadratic equation,

$$p_4=\frac{1}{2(E_{45}^2-P_{45}^2\cos^2\alpha)}\times\{P_{45}\cos\alpha\epsilon_{45}^2+E_{45}\times[\epsilon_{45}^4-4m_4^2(E_{45}^2-P_{34}^2\cos^2\alpha)]^{1/2}\}\ ,$$

where $\epsilon_{45}^2=M_{45}^2+m_4^2-m_5^2$, and α is the polar angle between the pion direction of flight (θ_4,φ_4) and $\mathbf{P}_{45}$. It follows immediately that $\mathbf{p}_5=\mathbf{P}_{45}-\mathbf{p}_4$.

The PWIA differential cross section has the well-known factorized form:

$$\frac{d^3\sigma}{dp_3 d\Omega_3 d\Omega_4}=K\,|\,\phi(p_5)\,|^2(d\sigma/d\Omega)^{\text{c.m.}}_{\text{pp}\to\text{d}\pi}\ , \tag{3.2}$$

where K is a kinematic factor including the necessary coordinate transformation and $(d\sigma/d\Omega)^{\text{c.m.}}_{\text{pp}\to\text{d}\pi}$ is the half-off-shell center-of-mass cross section for $\text{pp}\to\text{d}\pi^+$ at the scattering vertex in Fig. 1(a). A number of methods have been used in the past to resolve the difficulty related to the off-shell property of the target nucleon in such a three-body reaction. The "final state" prescription is usually chosen; then $(d\sigma/d\Omega)^{\text{c.m.}}_{\text{pp}\to\text{d}\pi}$ is replaced by the free cross section at an energy defined by $s=M_{45}^2=(p_3+p_4)^2$ and at an angle defined by the invariant four-momentum transfer squared, $t=(p_1-p_4)^2$ [see Eqs. (3.3a) and (3.3b) below]. Finally, in Eq. (3.2) the quantity $|\,\phi(p_5)\,|^2$ is the single-proton momentum density distribution. It is the determination of this quantity which is the primary goal of the data analysis of the present experiment.

As p_5 is the variable of interest in the PWIA, one does want to assign a value of p_5 to each data point defined by Eq. (3.1). However, this procedure will be correct only in the limit of vanishingly small intervals Δp_3, $\Delta\Omega_3$, and $\Delta\Omega_4$. For a finite phase space volume, small values of p_5, and when the momentum distribution $|\,\phi(p_5)\,|^2$ varies rapidly, as is the case for the deuteron, the discrepancy between p_5 calculated from the kinematical variables and the most likely p_5 can become very large. One can handle this effect as a resolution correction; or perform a complete simulation of the experiment by the Monte Carlo method and directly calculate the phase space volume element in Eq. (3.1) for each data point. Yet another possibility was proposed recently by Stetz,[9] and is the method we have used here. This particular choice of the five variables to be calculated from the measured values $(\mathbf{p}_3,\theta_4,\varphi_4)$ includes three relativistic invariants:

$$s=M_{34}^2=(p_3+p_4)^2=m_1^2+m_6^2+2E_{\text{coll}}m_6\ , \tag{3.3a}$$

$$t=(p_1-p_4)^2=m_1^2+m_4^2-2(E_{\text{c.m.}}^2-p_{\text{c.m.}}^2\cos\delta)\ , \tag{3.3b}$$

$$u=(p_2-p_5)^2=m_2^2+m_5^2-2E_5m_2\ , \tag{3.3c}$$

and the two azimuthal angles ψ and ξ defined in Fig. 4. The data must be ξ independent when the target is not polarized, as well as ψ independent as a direct consequence of the IA (Yang-Treiman angle[10]). The present data, containing only nearly coplanar events, do not allow a test of the ψ independence; consequently the data analysis assumes ψ independence. Formulas (3.3a) and (3.3b) above

also give the definition of the collision energy $E_{\rm coll}$ (m_6 is the physical mass of the struck proton) and c.m. scattering angle, δ, corresponding to the final state prescription. Formula (3.3c) establishes the relation of the variable u to the neutron recoil momentum $p_5=(E_5^2-m_5^2)^{1/2}$. This choice of variables is particularly well suited for a PWIA analysis because three of the variables, the three relativistic invariants, appear directly in the IA cross section, which now has the form:

$$\frac{d^5\sigma}{ds\,dt\,du\,d\psi\,d\xi}=\frac{\pi E_5 s^{1/2}}{2p_1m_2E_6P_{34}p^{\rm c.m.}}\,|\phi(p_5)|^2 \times(d\sigma/d\Omega)^{\rm c.m.}_{\rm pp\to d\pi}\,, \tag{3.4}$$

where $E_6=(p_5^2+m_6^2)^{1/2}$ and $p^{\rm c.m.}$ is the momentum in the center of mass of particles 3 and 4 determined by the invariant energy $s^{1/2}$, and all other quantities have been defined previously.

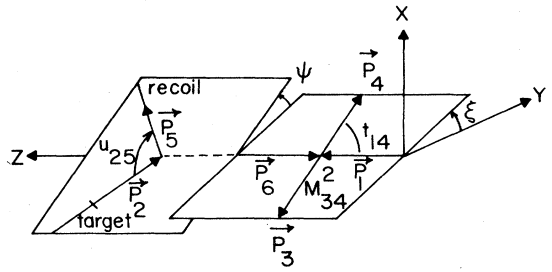

FIG. 4. Definition of the azimuthal angles ψ and ξ in the collision frame for $1+6\to3+4$. The z axis is not in the beam direction, but along $\mathbf{p}_1+\mathbf{p}_6=\mathbf{p}_1-\mathbf{p}_5$, and therefore is different for each reaction event.

With the variables defined by Eqs. (3.3a)—(3.3c), the definition of the cross section Eq. (3.1) must be changed to:

$$\frac{d^5\sigma}{ds\,dt\,du\,d\psi\,d\xi}=\frac{1}{4\pi m_2\Delta p_5\Delta(\cos\theta_4)\Delta M_{34}}\frac{1}{nI\epsilon}\left\{\sum_{i=1}^{N}\left[\frac{E_5}{(\partial t/\partial\cos\theta_4)M_{34}\epsilon_\pi}\frac{1}{\int d\psi\,d\xi}\right]_i\right\}, \tag{3.5}$$

where the term within [ ] is the sum over all events, N, in a given interval of p_5, θ_4, and M_{34}. The argument of the sum varies from event to event. The integral $\int d\psi\,d\xi$ over the boundaries of the detectors is evaluated event by event using a numerical method proposed by Stetz (for details see Debebe[11]). The term outside [ ] in Eq. (3.5) is the same for all events and n, I, ϵ, and ϵ_π have the same definition as in Eq. (3.1).

In Sec. IV the results of this experiment will be presented in the form of cross sections as defined by Eq. (3.5), and momentum densities $|\phi|^2$ obtained from Eq. (3.4). The pp$\to$dπ cross section input used is the parametrization of Spuller and Mesday,[12] that is, for the angular distribution:

$$(d\sigma/d\Omega)^{\rm c.m.}_{\rm pp\to d\pi}=K_p(A_0+\cos^2\delta-A_2\cos^4\delta) \tag{3.6}$$

with $A_0=0.21\,(1+\alpha/\beta\eta^2)$ and $A_2=0.25$. In Eq. (3.6) η is the c.m. pion momentum in units of the pion mass. Values of $\alpha=0.27$ and $\beta=0.55$ were used. The total cross section is then:

$$\sigma_{\rm pp\to d\pi}=4\pi K_p[A_0+\tfrac{1}{3}-(\tfrac{1}{5})A_2]\,,$$

where the value of K_p is determined from the energy dependence fit:

$$\sigma_{\rm pp\to d\pi}=\alpha\eta-0.2\eta^2+\beta\eta^3+\eta^4-\beta\eta^5\,. \tag{3.7}$$

IV. RESULTS OF THE EXPERIMENT

The complete results of this experiment can be obtained in table form from the authors. The cross sections $d^5\sigma/ds\,dt\,du\,d\psi\,d\xi$ for deuteron angles (MRS) of 11°, 13°, 15°, and 17° are shown in Figs. 5—10 as a function of neutron recoil momentum p_5. In these figures, the different symbols used refer to the pion angle; the data shown include pion angles between 24° and 96° in steps of 8°. Additional data at 28°, 36°, 44°, and 55° have been left out of the figures but are in the tables. At the deuteron angle of

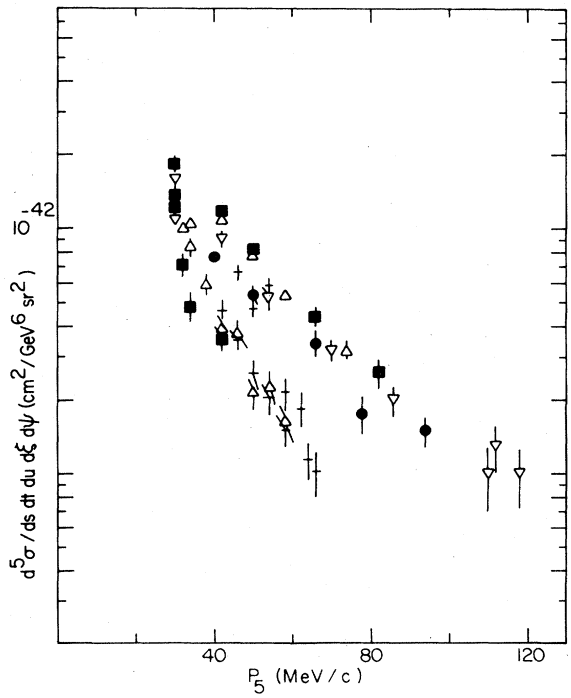

FIG. 5. Cross section $d^5\sigma/ds\,dt\,du\,d\xi\,d\psi$ for the deuteron angle 11° and central momentum 860 MeV/c. The pion angles are shown with (+) for 24°; (Δ), for 32°; (■), for 40°; (▽), for 48°; (●), for 56°; (×), for 64°; (▲), for 72°; (□), for 80°; (▼), for 88°; and (○), for 96°.

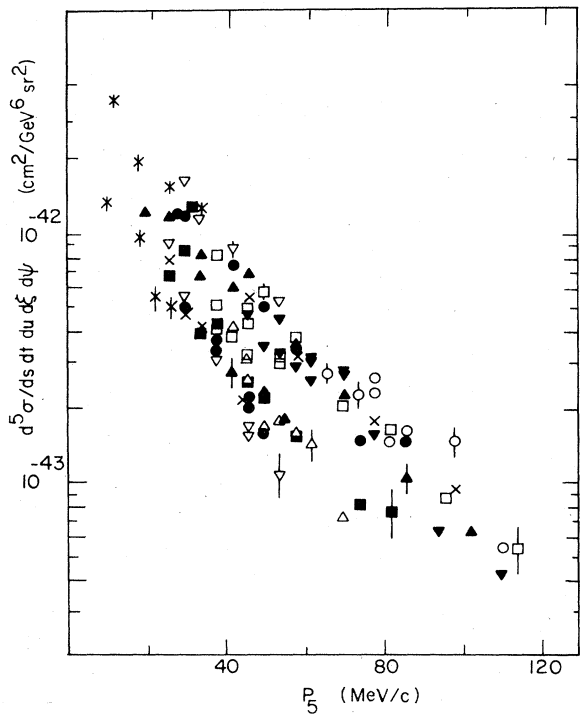

FIG. 6. Cross section $d^5\sigma/ds\,dt\,du\,d\xi\,d\psi$ for the deuteron angle 11° and central momentum 979 MeV/c. Symbols for the pion angles as in Fig. 5.

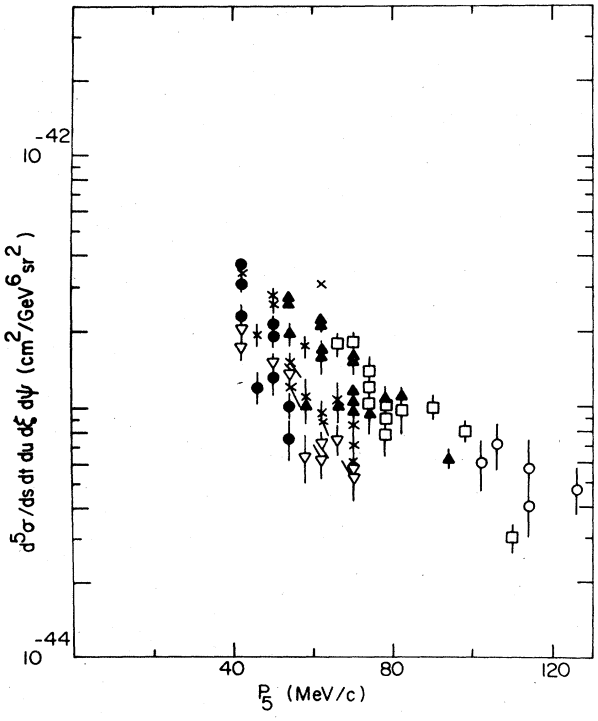

FIG. 8. Cross section $d^5\sigma/ds\,dt\,du\,d\xi\,d\psi$ for the deuteron angle 13° and central momentum 1054 MeV/c. Symbols for the pion angles as in Fig. 5.

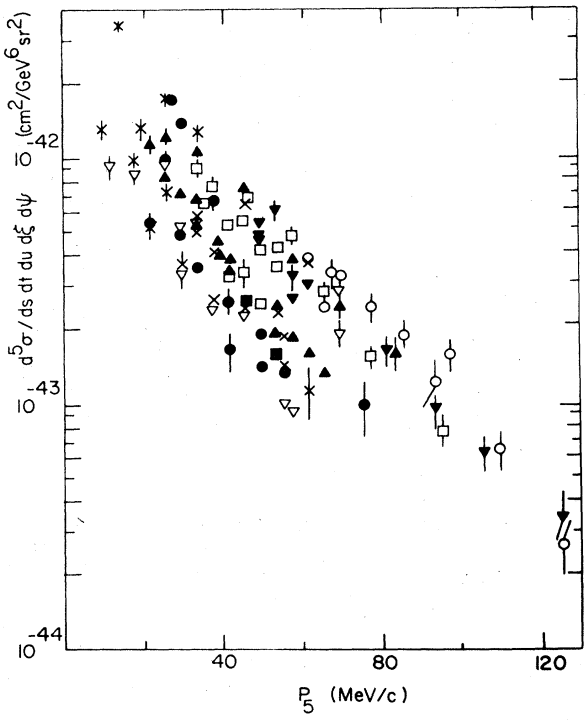

FIG. 7. Cross section $d^5\sigma/ds\,dt\,du\,d\xi\,d\psi$ for the deuteron angle 11° and central momentum 1053 MeV/c. Symbols for the pion angles as in Fig. 5.

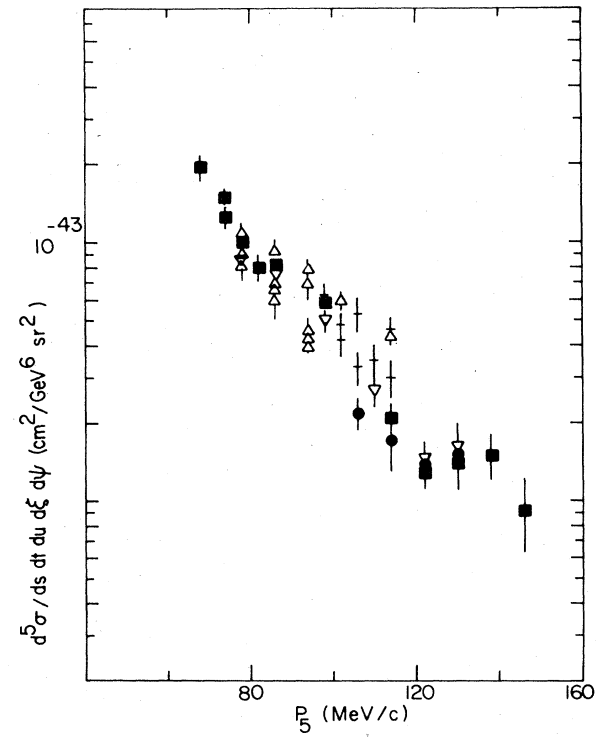

FIG. 9. Cross section $d^5\sigma/ds\,dt\,du\,d\xi\,d\psi$ for the deuteron angle 15° and central momentum 789 MeV/c. Symbols for the pion angles as in Fig. 5.

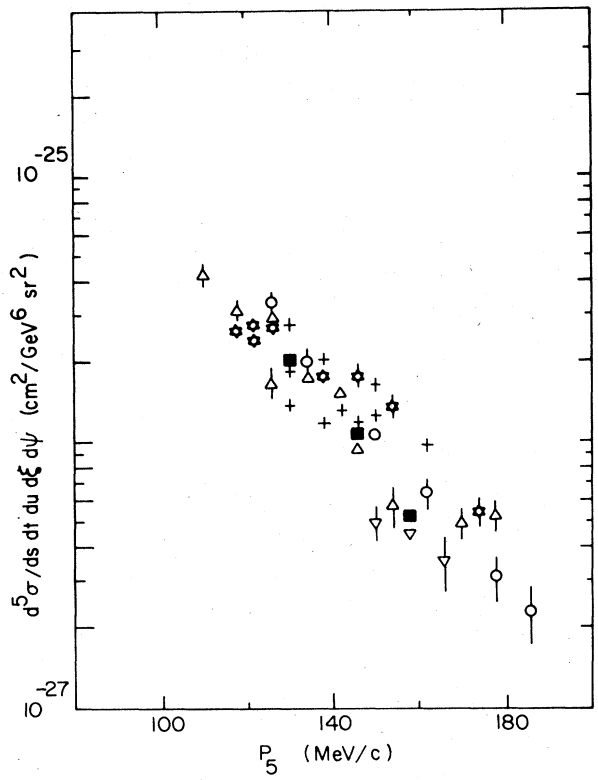

FIG. 10. Cross section $d^5\sigma/ds\,dt\,du\,d\xi\,d\psi$ for the deuteron angle 17° and central momentum 708 MeV/c. Symbols for the pion angles as in Fig. 5, (✡) for 28°.

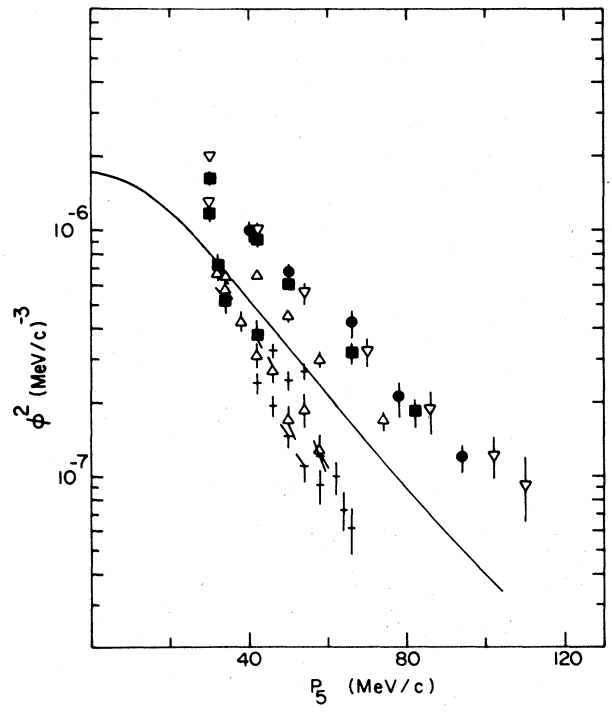

FIG. 11. PWIA internal momentum distribution $|\phi(p_5)|^2$ for the deuteron angle of 11°, data from Fig. 5. Symbols for the pion angles as in Fig. 5. The curve represents the Paris potential deuteron distribution.

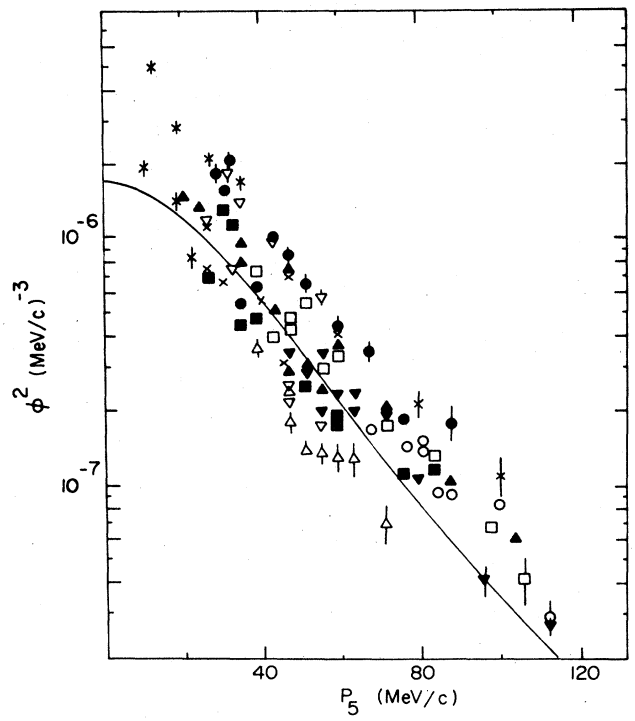

FIG. 12. PWIA internal momentum distribution $|\phi(p_5)|^2$ for the deuteron angle 11°, data from Fig. 6 and symbols from Fig. 5. Curve represents Paris potential.

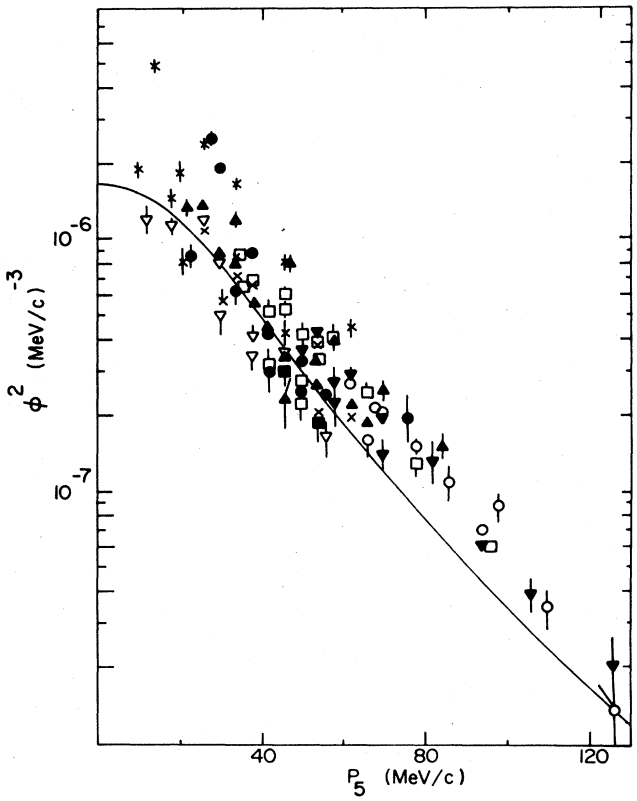

FIG. 13. PWIA internal momentum distribution $|\phi(p_5)|^2$ for the deuteron angle 11°, data from Fig. 7 and symbols from Fig. 5. Curve represents Paris potential.

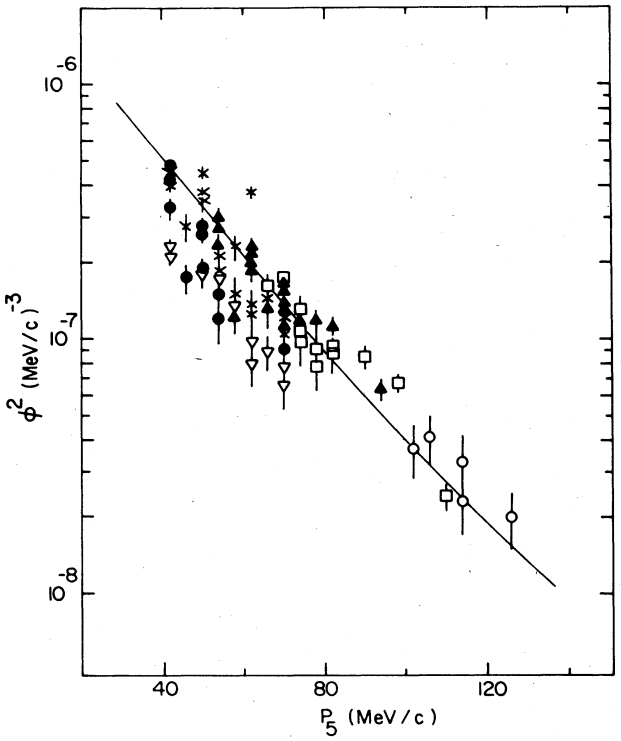

FIG. 14. PWIA internal momentum distribution $|\phi(p_5)|^2$ for the deuteron angle 13°, data from Fig. 8 and symbols from Fig. 5. Curve represents Paris potential.

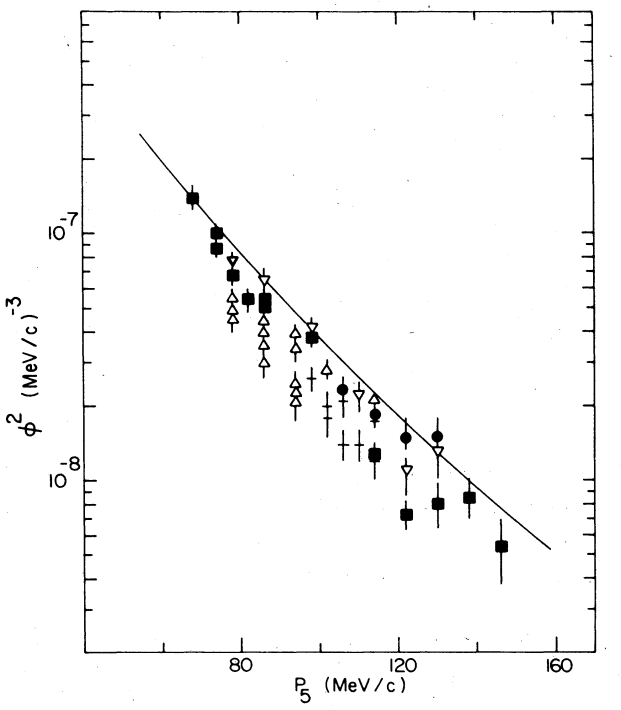

FIG. 15. PWIA internal momentum distribution $|\phi(p_5)|^2$ for the deuteron angle 15°, data from Fig. 9 and symbols from Fig. 5. Curve represents Paris potential.

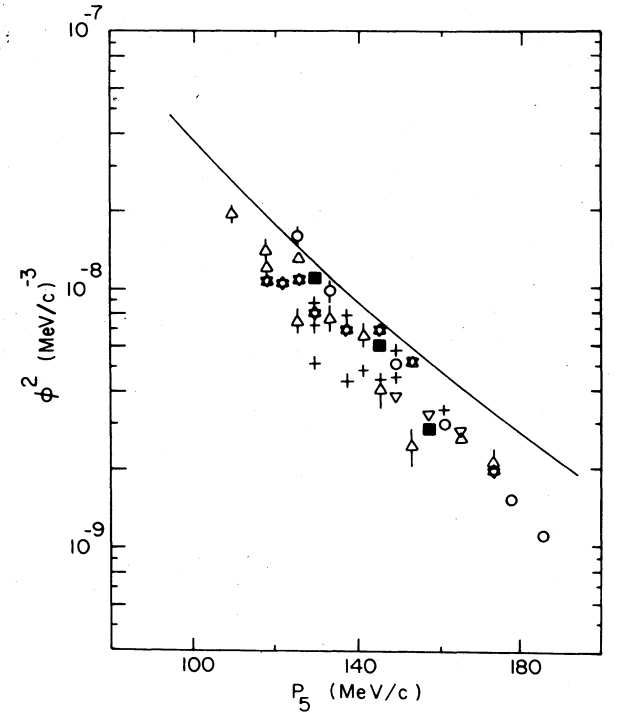

FIG. 16. PWIA internal momentum distribution $|\phi(p_5)|^2$ for the deuteron angle 17°, data from Fig. 10 and symbols from Fig. 10. Curve represents Paris potential.

11°, the data for three central values of the deuteron momentum $\bar{p}_3$ are shown separately in Figs. 5–7 for $\bar{p}_3 = 860$, 979, and 1053 MeV/c, respectively. Only one value of the central deuteron momentum is included at the other deuteron angles in Figs. 8–10 (1054, 789, and 708 MeV/c, respectively); data at two additional central deuteron momenta have also been obtained at each one of the three larger deuteron angles.

The error bars shown in Figs. 5–10 are statistical only. The overall systematic uncertainty, including contributions from solid angle definition, target thickness, orientation and composition, polarimeter calibration, and multiple scattering losses is estimated to be 15% and applies to all data points.

The proton momentum densities calculated from the cross sections in Figs. 5–10 using the PWIA as explained in Sec. III are shown in Figs. 11–16 and will be discussed in the next section.

V. DISCUSSION OF THE RESULTS

A. Comparison with the PWIA

Many reactions in the intermediate energy regime, including (p,2p), (e,e'p), (π,π'p), (α,2α), ..., have been analyzed in terms of the PWIA and for target nuclei with up to four nucleons, the momentum distributions extracted have in general corresponded to theoretical expectation. Although both shape and magnitude of the experimental single nucleon momentum distributions are generally understood below 200 MeV/c recoil momentum, the data at

larger recoils are systematically in excess of theory, with the exception of the electron data. Recent (p,2p) (Ref. 3) and (e,e'p) (Ref. 13) experiments on the deuteron, analyzed in PWIA, have given $|\phi|^2$ distributions corresponding closely to the Paris[14] and Bonn[15] deuteron wave functions, although the data suggest the need for an attenuation factor of 0.8 to 0.9. A recent review of the electron data is found in Frullani and Mougey.[16] Results of Bracco *et al.*[17] and van Oers *et al.*[18] for (p,2p) on ^{3}He and ^{4}He, respectively, also give $|\phi|^2$ distributions in good agreement with theory up to 200 MeV/c.

It is common in all these experiments to measure a number of data points, each corresponding to a different value of the recoil momentum p_5, sometimes at a few beam energies. In the present experiment we have deliberately obtained data which, for a given value of p_5, extend over a significant range of values for the other two physically interesting kinematical variables (for example t and M_{34} or M_{45}) at one beam energy. Our results for $|\phi|^2$, as seen in Figs. 11–16, do show that the PWIA is not valid to within better than a factor of about 3 in the ^{2}H(p,dπ^+)n reaction at 506 MeV: Instead of a single value of $|\phi|^2$ for a given neutron momentum we observe a clustering of the data around two values of $|\phi|^2$. Most visibly in Figs. 11–14 the data are scattered along a looping locus with $|\phi|^2$ at a given p_5 systematically smaller at small pion angle than at large pion angle. To illustrate this point, the data of Fig. 11 are shown again, but schematically, in Fig. 17. The double valuedness of $|\phi|^2$ is clearly visible, as well as its correlation with the pion angle, or the collision energy $s^{1/2}=M_{34}$ [see formula (3.3a)]. Starting for example at point A, the smallest pion angle ($\theta_4=24°$), M_{34} systematically increases from 2.100 to 2.125 GeV at point B and 2.155 GeV at C. At B, where the minimum recoil occurs with neutron and pion momenta parallel to each other, the value of M_{34} is 55 MeV below the (3,3) resonance at the pp$\rightarrow$dπ^+ vertex of Fig. 1(a). The dependence of $|\phi|^2$ on variables other than p_5 is in direct violation with the PWIA prediction that it should be a unique function of p_5.

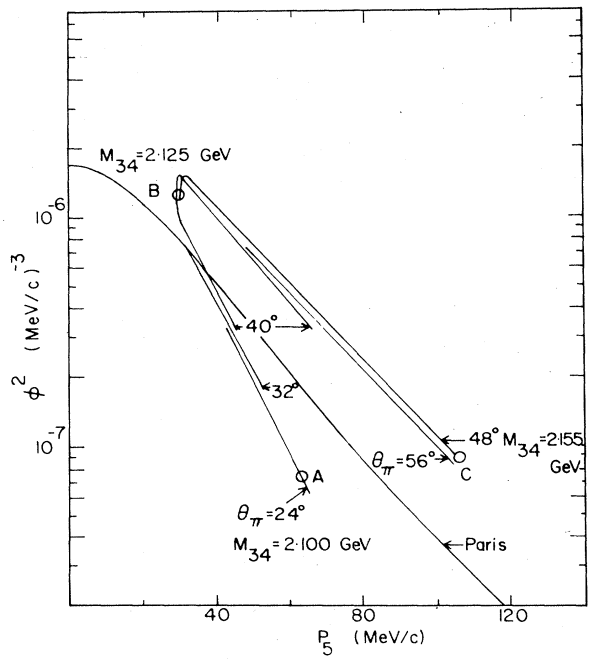

FIG. 17. Schematic rendering of the distribution of Fig. 11 with indication of the pion angles and of the collision energy M_{34}. Also shown is the Paris potential distribution.

The only other experiment which has been performed in a way to allow exploration of a significant region of the final state phase space is that of ^{2}H(p,dπ^+)n by Lo *et al.*[5] at 800 MeV. Although these authors did not present their results in the form of a $|\phi|^2$ distribution, their data show a behavior very similar to that seen in Fig. 17, both for the cross sections and $|\phi|^2$ values. In Ref. 4, in which the range of neutron recoils is 5–120 MeV/c, the ratio of $|\phi|^2$ in the two branches is typically 1.8, to be compared with 3.0 for the present data.

Before we attempt to interpret the characteristic behavior illustrated in the $|\phi|^2$ distribution of Figs. 11–14 in terms of rescattering corrections to the PWIA, a discussion of the possibility that the present results are due either to instrumental distortion or improper assumptions in calculation of the PWIA is in order. Instrumental effects have been studied with the help of a complete simulation of the experimental geometry and reaction kinematics using the Monte Carlo method; however, as explained in Sec. III A, no attempt was made to calculate directly the phase space acceptance of the experiment. Events were generated with uniform population of either the (p_3,cosθ_3,ϕ_3,cosθ_4,ϕ_4) phase space (θ and ϕ stand here for spherical angles of particles 3 and 4), or of the (s,t,u,ψ,ξ) phase space. Details of the variable transformations required when the second set of variables is used can be found in Ref. 11. Each event was then given a weight depending upon the magnitude of p_5 determined by the choice of the primary variables. The resulting phase space population data were then treated the same way as the experimental data, using Eqs. (3.2) and (3.3) to extract the $|\phi|^2$ distribution. The results show no indication of double valuedness in either representation, ruling out a geometrical effect as the origin of the splitting into two branches observed in the experiment.

Another possible cause for the disagreement between data and PWIA might be the approximation implied when the half-off-shell amplitude at the scattering vertex in Fig. 1(a) is replaced by an on-shell cross section in Eq. (3.4). However, under the conditions of this experiment, both the binding energy of the deuteron (2.22 MeV) and the low values of the neutron recoil momenta (typically 60 MeV/c) ensure that the struck proton [particle 6 in Fig. 1(a)] is not far from the mass shell. We see significant deviations from the PWIA when the proton is off the mass shell by 5 MeV. As pointed out earlier, $|\phi|^2$ for a given neutron recoil momentum tends to be larger at the larger pion angles. That might suggest that the angular dependence of the pp$\rightarrow$dπ^+ cross section used in Eq. (3.4), which we have approximated by Eq. (3.6), is incorrect. However, since the struck proton is not far off shell, the pion angle calculated from Eq. (3.3b) is never significantly different from the observed angle. Figure 17 shows clearly that $|\phi|^2$ increases abruptly when we pass through the

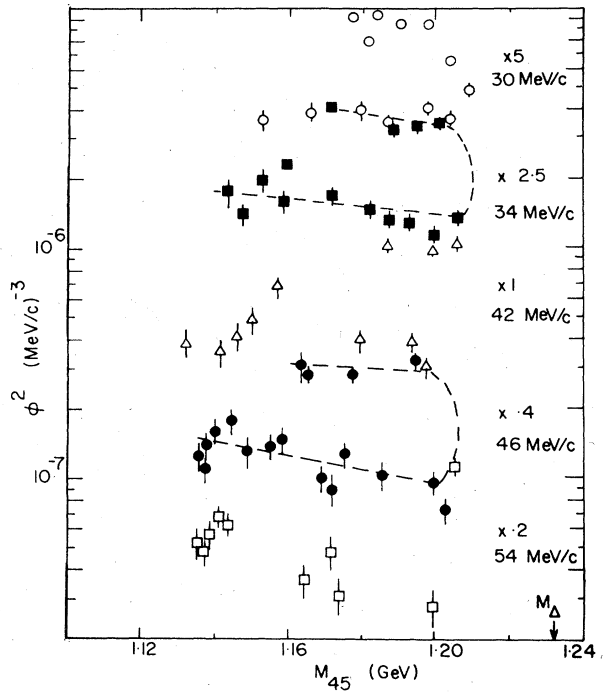

FIG. 18. Selected data from Fig. 11 shown for five values of the neutron recoil momentum as a function of M_{45}, the invariant mass of the πn pair. Data at the pion angles of 28°, 36°, 44°, and 52° have also been included here.

minimum recoil kinematics at point *B*, where the energy in the πd pair is 55 MeV below the (3,3) resonance. The $pp\rightarrow d\pi^+$ total cross section has a prominent maximum at the (3,3) resonance, and the present data can be interpreted as indicating that, in the presence of the neutron, the $pp\rightarrow d\pi^+$ process resonates at a smaller energy than in the free reaction. Similar shifts of the (3,3) resonance are known to occur in two-body reactions like $\gamma d\rightarrow pn$ and $pd\rightarrow t\pi^+$. For the three-body reaction of interest here, significant contributions from rescattering processes might cause such a shift. To investigate this point, a calculation of the cross section for nd rescattering was done and is presented in Sec. IV B. No calculation of the π^+n rescattering graph of Fig. 1(c) was done. Isospin conservation selects the $I=\frac{1}{2}$ state for the π^+n system and at the typical neutron energy of 22 MeV the total $I=\frac{1}{2}$ cross section for π^+d is only 10 mb, much smaller than the total elastic nd cross section which is found to be 370 mb by integrating the data of Bunker *et al.*[19] Thus nd rescattering should be more important than π^+n rescattering. Rescattering in the π^+n channel might manifest itself as a characteristic dependence of the cross section, and therefore of the $|\phi|^2$ distribution upon M_{45}. In Fig. 18 $|\phi|^2$ is shown as a function of M_{45} for five values of the neutron recoil momentum p_5. The value $M_{45}=1.232$ GeV corresponds to the (3,3) resonance in free πN. The double valuedness of $|\phi|^2$ is apparent. The abrupt transition from a low value of $|\phi|^2$ to a high value occurs near the maximum value of M_{45} reached, which is 1.210 GeV. Note that M_{45} is a maximum when $\mathbf{p}_4$ and $\mathbf{p}_5$ are parallel, which is also the condition for the magnitude of $\mathbf{p}_5$ to be a minimum. At constant neutron recoil, $|\phi|^2$ show no enhancement as M_{45} approaches the (3,3) resonance value. On the contrary, a slight but systematic decrease of $|\phi|^2$ for increasing M_{45} might be present.

To conclude the discussion of the results of this experiment in terms of the PWIA values of $|\phi|^2$, we point out that at the deuteron angle of 11° the Paris potential (Ref. 14) momentum density goes right through the middle between the two branches, as seen in Figs. 11–13. The same would be true for the Bonn potential of Ref. 15. For increasing deuteron angle the Paris momentum density tends to become increasingly larger than the experimental results, as seen in Figs. 14–16.

B. Neutron-deuteron rescattering calculation

A calculation of the cross section corresponding to the triangular graph of Fig. 1(b) was made following the method of Laget as outlined in Ref. 5 for πp and NN rescattering in the reaction $\gamma^2\mathrm{H}\rightarrow\mathrm{NN}\pi$. The matrix element for single nd rescattering is written in the form:

$$|\mathcal{M}|^2=\tfrac{1}{18}\sum|\mathcal{M}_{d\pi}|^2\sum|\mathcal{M}_{nd}|^2\left[\int\frac{d^3q}{(2\pi)^3}\frac{1}{\sqrt{4\pi E_q}}\frac{\phi(q)}{p_3^2-m_3^2+i\epsilon}\right], \tag{5.1}$$

where q is the Fermi momentum at the $d\rightarrow pn$ vertex. $\mathcal{M}_d^2$ and $\mathcal{M}_{nd}^2$, the elementary amplitudes squared at the $pp\rightarrow d\pi$ and $nd\rightarrow nd$ vertices, have been taken out of the integral and will be evaluated at $q=0$. The integral over the angular variables and the magnitude of $\mathbf{q}$ is calculated analytically using the McGee[20] parametrization for the deuteron *S*-state wave function:

$$\phi(q)=4\pi N\sum_{j=0}^{4}\frac{C_j}{q^2+\alpha_j^2},$$

where N is the normalization constant and the α_j's have been determined to fit the Hamada-Johnson[21] wave function. The result of the integration is then:

$$4\pi N^2\sum_j C_j\left[-\frac{i}{2}\ln\frac{(q^{\max})^2+\alpha_j^2}{(q^{\min})^2+\alpha_j^2}+\arctan\left[\frac{\alpha_j}{q^{\max}}\right]+\arctan\left[\frac{\alpha_j}{q^{\min}}\right]\right], \tag{5.2}$$

where $q^{\min}$ and $q^{\max}$ correspond to the neutron and deuteron momenta being parallel and antiparallel, respectively. The imaginary term is for on-shell propagation of the virtual deuteron, and the real part for off-shell propagation, respectively. For the conditions of this experiment the off-shell contribution always dominates; near $q=0$ the two off-shell terms nearly cancel. Away from $q=0$

the largest contribution comes from the $q^{\min}$ term in Eq. (5.2).

To evaluate $\mathcal{M}^2_{d\pi}$ in Eq. (5.1) we used the same parametrization as for the data analysis, Eqs. (3.6) and (3.7). $\mathcal{M}^2_{nd}$ was evaluated from the elastic nd cross section of Bunker *et al.*[19] and other data compiled in this work. A considerable amount of interpolation and extrapolation was necessary to obtain the cross sections for the conditions of our data. Thus the results in Fig. 19 must be considered mostly for their qualitative value. To facilitate comparison with the data, the calculation results in Fig. 19 are in the form of an effective $|\phi|^2$ obtained from Eq. (3.2). The calculated $|\phi|^2$ show a strikingly similar separation into two branches to that of the data, the small pion angle results being in the lower branch and the large pion angles in the upper branch. However the branch splitting is too large and the p_5 dependence does not match that of the data. The splitting is directly related with the change of regime from backward (lower branch) to forward (upper branch) nd scattering, which of necessity occurs near the minimum recoil condition imposed by the geometry of the detectors. The passage from the lower to the upper branch is abrupt because the kinematics change rapidly near the condition of minimum recoil and because nd scattering has a very strong angular dependence.

To conclude, it appears that the systematic departure from the PWIA revealed by the new data can, at least qualitatively, be explained in terms of nd rescattering. A better calculation should be done with the pp→dπ and nd→nd amplitudes not taken out of the integral in Eq. (5.1); both terms have a strong dependence upon the collision energy.

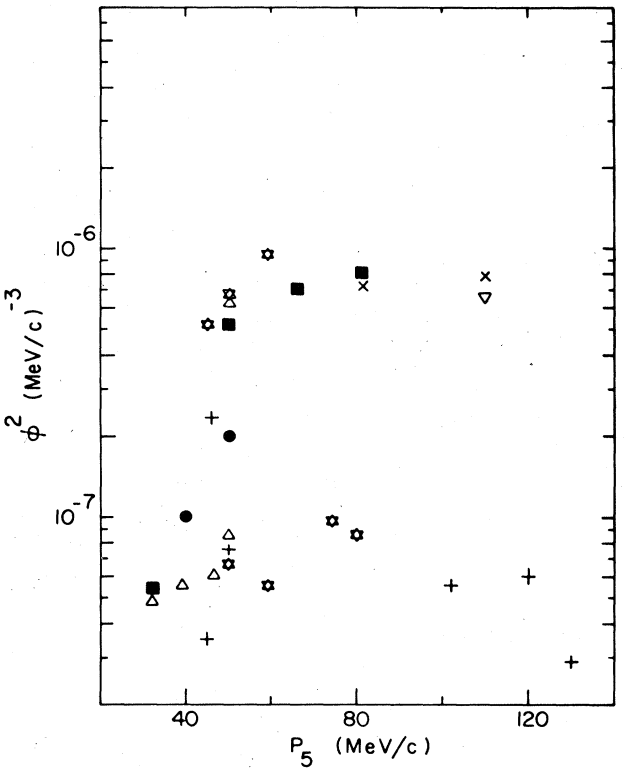

FIG. 19. Results of the calculation of the rescattering cross section shown as an equivalent internal momentum distribution obtained from Eq. (3.2). The deuteron angle and central momentum are 11° and 860 MeV/c, respectively. The symbols for the various pion angles are the same as in Fig. 5, with additionally 28° shown as (✡).

VI. CONCLUSIONS

New data for the reaction ^{2}H(p,dπ^+)n at 506 MeV have been obtained and analyzed in the framework of the plane wave impulse approximation (PWIA), in the domain of small neutron recoil momenta. The proton internal momentum distributions $|\phi(p_5)|^2$, where p_5 is the neutron recoil and therefore, in the IA, also the internal momentum of the struck proton, show a systematic double valuedness. This effect is not compatible with the PWIA; it is most visible when the deuteron angle is 11°. A similar behavior has been observed in the 800 MeV data of Ref. 4 for the same reaction. Because the π^+n pair in the final state is constrained by isospin conservation to the isospin $\frac{1}{2}$ state, the (3,3) resonance should not be important in the rescattering graph of Fig. 1(c). The possibility that rescattering within the nd pair is at the origin of the disagreement with the PWIA is discussed. The calculated cross sections for the nd rescattering process of the graph in Fig. 1(b) are comparable in size to the PWIA ones. The typical double valuedness seen in the data is reproduced. It has its origin in the largely different amplitudes for forward and backward nd scattering. The calculated splitting is too large at the deuteron angle of 11°. However, for increasing deuteron angles, the nd collision energy increases and therefore the rescattering cross section decreases, in agreement with the data. A quantitative comparison with the data will necessitate the evaluation of other rescattering diagrams. The importance of single rescattering suggests that higher order processes might also have to be evaluated.

ACKNOWLEDGMENTS

We wish to thank the technical staff at TRIUMF for their help during the data acquisition phase of this work, and particularly D. A. Hutcheon and R. Abegg. Also, we are thankful for the invaluable help received from the staff at the William and Mary computer Center. This work was supported in part by the Natural Sciences and Engineering Research Council of Canada and the U.S. National Science Foundation.

*Present address: Physics Department, University of Massachusetts, Amherst, MA 01003.

†Present address: SWITCO Inc., 385 Nordhoff Place, Englewood, NJ 07601.

‡Permanent address: University of the Western Cape, Bellville, 7530, Republic of South Africa.

§Now at TRIUMF, Vancouver, British Columbia, Canada V6T 1W5.

**Present address: 9345-98 A Street, Edmonton, Alberta, Canada T6E 3N2.

††Now at Defense Research Establishment Pacific; F. M. O. Victoria, British Columbia, Canada V0S 1B0.

[1]H. W. Fearing, TRIUMF Report TRI-PP-81-61, 1981 (unpublished).

[2]P. Walden, in *High Energy Physics and Nuclear Structure,* edited by P. Catillon, P. Radvanyi, and M. Porneuf (North-Holland, Amsterdam, 1982), p. 277c.

[3]C. F. Perdrisat, L. W. Swenson, P. C. Gugelot, E. T. Boschitz, W. K. Roberts, J. S. Vincent, and J. R. Priest, Phys. Rev. **187**, 1201 (1969); T. R. Witten, M. Furic, G. S. Mutchler, C. R. Fletcher, N. D. Gabitzsch, G. C. Phillips, J. Hudomalj, L. Y. Lee, B. W. Mayes, J. Allred, and C. Goodman, Nucl. Phys. **A254**, 269 (1975); R. D. Felder, T. R. Witten, T. M. Williams, M. Furic, G. C. Mutchler, N. D. Gabitzsch, J. Hudomalj-Gabitzsch, J. M. Clement, Jr., G. C. Phillips, E. V. Hungerford, L. Y. Lee, M. Warnecke, B. W. Mayes, and J. C. Allred, *ibid.* **A264**, 397 (1976).

[4]J. M. Laget, Nucl. Phys. **A296**, 388 (1978).

[5]J. W. Lo, E. V. Hungerford, J. C. Allred, B. W. Mayes, L. S. Pinsky, M. L. Warnecke, T. M. Williams, J. M. Clement, W. H. Dragoset, R. D. Felder, J. H. Hoftiezer, J. Hudomalj-Gabitzsch, G. S. Mutchler, and G. C. Phillips, Phys. Rev. C **20**, 1479 (1979).

[6]K. R. Hogstrom, G. S. Mutchler, T. R. Witten, J. Hudomalj-Gabitzsch, J. M. Clement, R. D. Felder, W. H. Dragoset, W. P. Madigan, J. A. Bachman, G. C. Phillips, E. V. Hungerford, B. W. Mayes, L. Pinsky, L. Y. Lee, T. M. Williams, and J. C. Allred, Phys. Rev. C **17**, 259 (1978).

[7]I. Duck, K. R. Hogstrom, and G. S. Mutchler, Phys. Rev. C **18**, 887 (1978).

[8]L. Antonuk, Ph.D. thesis, University of Alberta, 1979 (unpublished).

[9]A. W. Stetz, Phys. Rev. C **21**, 1979 (1980).

[10]C. N. Yang and S. Treiman, Phys. Rev. Lett. **8**, 140 (1962).

[11]B. Debebe, Ph.D. thesis, College of William and Mary, 1983 (unpublished).

[12]J. Spuller and D. F. Mesday, Phys. Rev. D **12**, 3550 (1975).

[13]M. Bernheim, A. Bussiere, J. Mougey, D. Royer, D. Tarnowski, S. Turck-Chieze, S. Frullani, G. P. Capitani, E. de Sanctis, and E. Jans, Nucl. Phys. **A365**, 349 (1981).

[14]M. Lacombe, B. Loiseau, R. Vinh-Mau, J. Cote, P. Pires, and R. de Toureil, Phys. Lett. **101B**, 139 (1981).

[15]R. Machleidt, TRIUMF Report TRI-PP-128, 1983 (unpublished).

[16]S. Frullani and J. Mougey, in *Advances in Nuclear Physics,* edited by J. Nagele and E. Vogt (Plenum, New York, 1984), Vol. 14, p. 1.

[17]A. Bracco, H. P. Gubler, D. K. Hasell, W. P. Lee, W. T. H. van Oers, M. B. Epstein, D. A. Krause, D. J. Margaziotis, R. Abegg, C. A. Miller, and A. W. Stetz, Phys. Lett. **137B**, 311 (1984).

[18]W. T. H. van Oers, B. T. Murdoch, B. K. S. Koene, D. K. Hasell, R. Abegg, D. J. Margaziotis, M. B. Epstein, G. A. Moss, L. G. Greeniaus, J. M. Greben, J. M. Cameron, J. G. Rogers, and A. W. Stetz, Phys. Rev. C **25**, 390 (1982).

[19]N. Bunker, J. M. Cameron, R. F. Carlson, J. Reginald Richardson, P. Tomas, W. T. H. van Oers, and J. W. Verba, Nucl. Phys. **A113**, 461 (1968).

[20]I. J. McGee, Phys. Rev. **151**, 772 (1966).

[21]T. Hamada and I. D. Johnson, Nucl. Phys. **34**, 382 (1962).